OPEN ACCESS

University of BRISTOL

Giordano, N., De Luca, F., & Sextos, A. (2020). Out-of-plane closed-form solution for the seismic assessment of unreinforced masonry schools in Nepal. *Engineering Structures*, *203*, [109548]. https://doi.org/10.1016/j.engstruct.2019.109548

Publisher's PDF, also known as Version of record

License (if available):
CC BY

Link to published version (if available):
10.1016/j.engstruct.2019.109548

Link to publication record in Explore Bristol Research
PDF-document

This is the final published version of the article (version of record). It first appeared online via Elsevier at https://www.sciencedirect.com/science/article/pii/S0141029619306650 . Please refer to any applicable terms of use of the publisher.

University of Bristol - Explore Bristol Research
General rights

This document is made available in accordance with publisher policies. Please cite only the published version using the reference above. Full terms of use are available:
http://www.bristol.ac.uk/red/research-policy/pure/user-guides/ebr-terms/

Engineering Structures 203 (2020) 109548

Contents lists available at ScienceDirect

Engineering Structures

journal homepage: www.elsevier.com/locate/engstruct

Out-of-plane closed-form solution for the seismic assessment of unreinforced masonry schools in Nepal

Nicola Giordano*, Flavia De Luca, Anastasios Sextos

Department of Civil Engineering, University of Bristol, Queen's Building, University Walk, Bristol, BS8 1TR, UK

ARTICLE INFO

Keywords:
Out-of-plane
Closed-form solution
Capacity curve
Vulnerability assessment
Unreinforced masonry
School buildings
Nepal

ABSTRACT

Traditional unreinforced masonry (URM) constructions still represent an important part of the school building stock in several low-income countries including Nepal. Unfortunately, their intrinsic vulnerability impacts negatively on the resilience of cities and local communities. Observations after major seismic events have shown that the predominant mode of failure is the out-of-plane (OOP) of the weak and loosely connected perimeter masonry walls which typically leads to partial or global collapse. Starting from this evidence, a closed-form analytical approach is presented aimed at deriving the OOP force-displacement response of URM walls for different boundary conditions and vertical loads. The novel analytical solution is successfully validated with the results of seventeen OOP experimental tests on URM walls available in the literature. Then, referring to a case-study Nepalese school building, capacity curves of the constituting walls are derived and adopted for the vulnerability assessment of the structure through the Capacity Spectrum Method (CSM) where equivalent hysteretic damping is calibrated with available OOP shaking table test results. Lastly, PGA capacities for different damage states are successfully compared with median values from observational fragility curves.

1. Introduction

In April 2015, a catastrophic M_W 7.8 earthquake followed by several aftershocks occurred in Nepal causing 8,790 deaths and 498,852 building collapses [1]. Particularly, the event significantly damaged the school facilities drawing the attention of Authorities to the high vulnerability of these buildings. According to different post-earthquake reconnaissance reports [2–6] approximately 6,000–8,200 schools were destroyed by the 2015 sequence of events. In terms of classrooms, 47,557 suffered structural damage of which 9.1% collapsed, while 5.1% and 7.8% experienced heavy and moderate damage [2].

Fortunately, the 2015 April 25th mainshock occurred on Saturday morning when school facilities were closed, therefore no causalities were recorded in these buildings. Given the level of damage and the amount of students living in the affected area (545,250 just in the Kathmandu Valley (KV), [7]), the number of fatalities could have been much higher if the earthquake had occurred during a weekday.

The structural configuration of most Nepalese school buildings (89%, [6]) consists of unreinforced masonry (URM) walls that bear both vertical and horizontal loads. In mountain areas at least 50% of them are effectively made of rubble-stone and dry or mud mortar joints. On the contrary, the construction practice in the KV is slightly different from the rest of the country thanks to the proximity to industrial activities and the availability of cement and bricks [8]. According to a study published by NSET and GeoHazards International [9] on the vulnerability of public schools in the KV, most of the school buildings were constructed between 1975 and 1995 with a consistent prevalence of URM walls made of brick and mud mortar. From 1995 onwards, an increase of brick with cement mortar masonry is reported. The vast majority of school buildings have only one or two stories with floors made of earth laid on wooden planks, supported by timber or bamboo joists [9].

From the standpoint of their seismic vulnerability, URM Nepalese schools are similar to residential and commercial buildings [9]. They are usually characterized by several structural weaknesses, as reported by Gautam et al. [1,10], Sharma et al. [11] and Brando et al. [12]. First, the floors commonly used in URMs cannot transfer the seismic forces to the vertical bearing structure due to their high in-plane flexibility and insufficient interlocking with bearing walls [10]. Secondly, there is a lack of wall-to-wall connection between orthogonal corner walls and seismic detailing (such as tie rods, anchors and ring beams) is commonly missing. Moreover, the quality of construction is poor, leading to insufficient seismic capacity [13–15].

For these reasons, Nepalese masonry buildings and, among them, school buildings, are not able to respond in a monolithic box-type manner under seismic actions [16,17], with the walls behaving

* Corresponding author.
E-mail address: nicola.giordano@bristol.ac.uk (N. Giordano).

https://doi.org/10.1016/j.engstruct.2019.109548
Received 18 February 2019; Received in revised form 8 July 2019; Accepted 12 August 2019
0141-0296/ © 2019 The Authors. Published by Elsevier Ltd. This is an open access article under the CC BY license (http://creativecommons.org/licenses/BY/4.0/).

Fig. 1. OOP damage of Nepalese URM buildings (credits: Rama Mohan Pokhrel).

independently and being particularly weak against transversal forces. This weakness was largely observed after the 2015 earthquake where out-of-plane (OOP) failure was the most critical damage [1,3–6,10–12] especially for low-axial load walls (i.e., non-loadbearing or at higher stories) (Fig. 1).

Given the above observations, the OOP response (conventionally represented by a force-displacement (*F-Δ*) diagram) is a key aspect for assessing the seismic vulnerability of Nepalese URM structures. Among the available approaches for *F-Δ* curves calculation [18], the present work focuses on analytical closed-form solutions. These are certainly more suitable in the context of Nepal since do not require specific structural analysis software. Additionally, although more advanced numerical/analytical approaches are available in the literature (e.g. [13,19–23]), closed-form solutions are still largely adopted thanks to their straightforward implementation. According to these methods, the wall is assumed as a rigid body that rotates around an overturning point, triggering the so-called collapse mechanism [24–27]. The simplification, firstly introduced by Heyman [28] and assumed in subsequent research works (e.g. [24,25,29]), allows the calculation of the *F-Δ* curve through a set of closed-form equations.

The main drawback of simplified methods is that *F-Δ* diagrams are represented by rough bilinear [28], trilinear [24,25] or quadrilinear [29,30] curves while laboratory tests shows smoother trends [31,32].

In this work, a novel non-piecewise-linear closed-form solution for the calculation of the OOP *F-Δ* curve of a masonry wall is presented (Section 2) and validated with respect to previous experimental tests (Section 3). Differently from most of the simplified methods available in the literature (e.g. [24,25,30,33]), this mechanical-based formulation directly accounts for the nonlinear behavior of the masonry wall at cross-section level, resulting in a more accurate matching with experimental results.

The proposed equations are adopted for the vulnerability assessment of a typical Nepalese masonry school building (Section 4). In line with the post-quake observations discussed above, the vulnerability assessment is based on three main assumptions: (i) the OOP failure mode is considered as the predominant damage pattern for traditional masonry constructions in Nepal [11,12]; (ii) the walls of the structure behave independently since no diaphragm action is guaranteed by the horizontal structures (i.e. floors and roof) [10]; (iii) as in D'Ayala et al. [34], the vulnerability of the whole building is ruled by the wall with the worst OOP seismic performance. The vulnerability assessment is based on the modified version of the Capacity Spectrum Method (CSM) proposed by Lagomarsino and Cattari [25,35]. Additionally, in the present study, one of the CSM ruling variables, i.e., the asymptote of the hysteretic damping $\xi_{h,MAX}$, is calibrated with respect to OOP shaking table test results available in the literature [27].

2. Evaluation of the out-of-plane capacity of masonry walls

The OOP capacity of a masonry wall is usually represented by a *F-Δ* curve. While this diagram can be calculated with a wide range of advanced techniques (refer to Ferreira et al. [18] for a detailed review), straightforward closed-form solutions are largely adopted for their low computational cost and fast applicability [29].

Three existing approaches for the derivation of piecewise linear *F-Δ* curves are reviewed. Subsequently, the novel mechanical-based closed-form solution is presented.

2.1. Existing simplified models for force-displacement curve estimation

2.1.1. Rigid body – Bilinear model

According to Heyman [28], a masonry wall (Fig. 2a) can be treated as a rigid body (cantilever configuration, Fig. 2b) or as a system of rigid bodies (with pinned-pinned, Fig. 2c, and clamped-clamped boundary conditions, Fig. 2d). Under this assumption, the *F-Δ* response is described by a *Bilinear model*. The first branch has infinite stiffness to represent perfectly-rigid behavior up to maximum lateral capacity. The second one is characterized by a negative slope until the attainment of the limit displacement before collapse (Fig. 3).

The maximum capacity F_0, i.e., the force at incipient rocking, and the limit top displacement Δ_{max} at collapse are directly evaluated by imposing the equilibrium in the generic deformed configuration. For instance, for the cantilever configuration (Fig. 2b) these parameters are defined as:

$$F_0 = \frac{(N + W)t}{2h\alpha_h}; \ \Delta_{max} = \frac{(N + W)t}{2(N + W/2)} \tag{1}$$

where N is the vertical load at the top of the wall, $W = B{\cdot}t{\cdot}h{\cdot}\gamma_m$ is its self-weight, B is the width, t is the thickness, h is the total height of the wall, γ_m is the masonry specific weight, and α_h is a non-dimensional coefficient ranging from 0 to 1, which defines the position of the resulting horizontal forceover the height of the wall.

2.1.2. Doherty et al. (2002) – Trilinear model

The model by Doherty at al. [24] starts from the rigid body approach to construct a trilinear *F-Δ* curve of the wall (Fig. 3). The two internal points of the *Trilinear model* are defined through the parameters $\{k_1, k_2\}$ that were evaluated from experimental results by the same authors [32]:

$$F_1 = F_2; \quad \Delta_1 = k_1\Delta_{max} \tag{2}$$

$$F_2 = (1 - k_2)F_0; \quad \Delta_2 = k_2\Delta_{max} \tag{3}$$

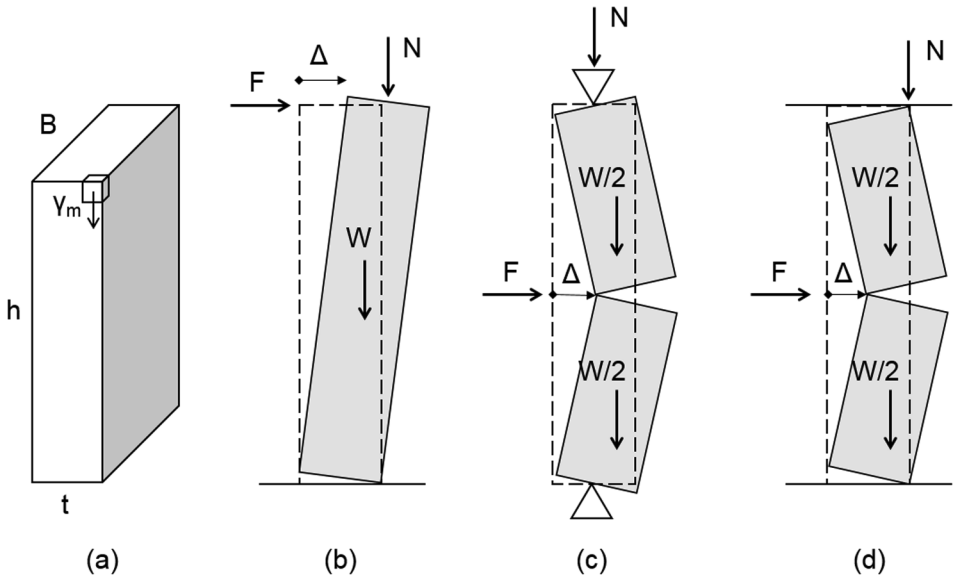

Fig. 2. (a) Masonry wall geometry. Boundary conditions: (b) cantilever (C); (c) pinned-pinned (P-P); (d) clamped-clamped (C-C).

2.1.3. Ferreira et al. (2015) – Quadrilinear model

The model of Ferreira et al. [29] is formulated to address the stability of a cantilever wall and it is characterized by a four branches *F-Δ* curve (*Quadrilinear model*). The first point of the curve corresponds to the cracking of the wall at the base:

$$F_{cr} = \frac{(N + W)t}{6h\alpha_h}; \quad \Delta_{cr} = \frac{(N + W)th^2}{18E_m I} \tag{4}$$

where E_m is the masonry Young's modulus and I is the cross-section inertia defined as $I = B{\cdot}t^3/12$. The post cracking branch is defined as:

$$F_y = \frac{\xi_s(N + W)t}{2h\alpha_h}; \quad \Delta_y = \frac{(N + W)th^2}{6E_m I\xi_k}\left(\xi_s + \frac{\xi_k}{3} - \frac{1}{3}\right) \tag{5}$$

where ξ_s and ξ_k are corrective parameters evaluated from experimental tests carried out by Ferreira et al. [33] with average values 0.92 and 0.67 respectively. The equations referred to the nonlinear plateau are:

$$F_I = F_y; \quad \Delta_I = 0.6(1 - \xi_s)t \tag{6}$$

While the last point of the curve is:

$$F_u = 0; \quad \Delta_u = 0.6t \tag{7}$$

2.2. Closed-form mechanical-based model

The mechanical-based model presented in this study is based on three main assumptions.

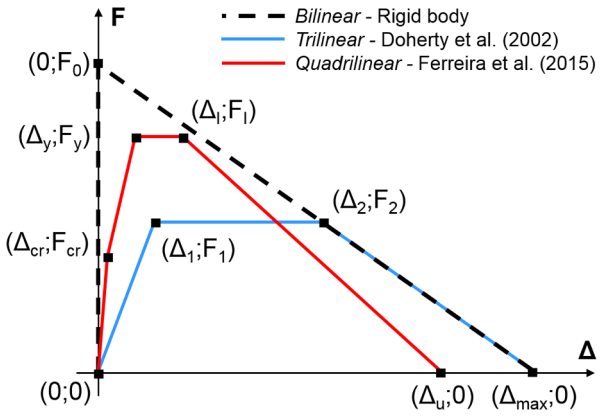

Fig. 3. *F-Δ* curves for different models.

i. The OOP response of a vertically spanning masonry wall is purely governed by bending (Fig. 4a). This hypothesis has been largely validated in experimental tests [27,31–33] and has been adopted in numerous mechanical-based models available in the literature [21–23,36].
ii. Since the nonlinear flexural deformations localize in the area with maximum bending moment (e.g., [31,33]), the wall is modeled as a rigid body connected to the ground with a nonlinear hinge (Fig. 4b).
iii. The moment-rotation relationship of the nonlinear hinge is computed starting from the moment-curvature (M-χ) of the critical cross-section (Fig. 4c). The M-χ curve is calculated under the assumption that axial strains behave linearly in bending; i.e., sections remain plane. This hypotheses has been largely discussed and validated, mostly in the works of Parisi et al. [37,38], Brencich at al. [39] and Cavaleri et al. [40]. In this study, the closed-form M-χ relationship reported by Giordano et al. [41] for the case of elastic-brittle no-tension masonry material is adopted. According to Crespi et al. [42], the uniaxial compressive limit is assumed equal to the strength of the masonry blocks f_{mb}. The rotation θ is calculated through a constant integration of the critical cross-section's curvature over the integration length L_i.

The model is adapted for the three boundary configurations previously discussed by introducing the quantity h_{LV}, i.e., the shear length of the wall:

$$\begin{cases} h_{LV} = h; & \text{(cantilever)} \\ h_{LV} = \frac{h}{2}; & \text{(pinned} - \text{pinned)} \\ h_{LV} = \frac{h}{4}; & \text{(clamped} - \text{clamped)} \end{cases} \tag{8}$$

The integration length L_i is assumed equal to $0.25{\cdot}h_{LV}$. This assumption is discussed in Section 3.3.

The first step required for the analytical formulation of the model is the definition of the moment-rotation relationship of the nonlinear hinge. As previously mentioned, this depends on the M-χ diagram of the critical cross-section. Giordano et al. [41] reported closed-form expression for a URM cross-section characterized by an elastic-brittle, no-tension material constitutive law:

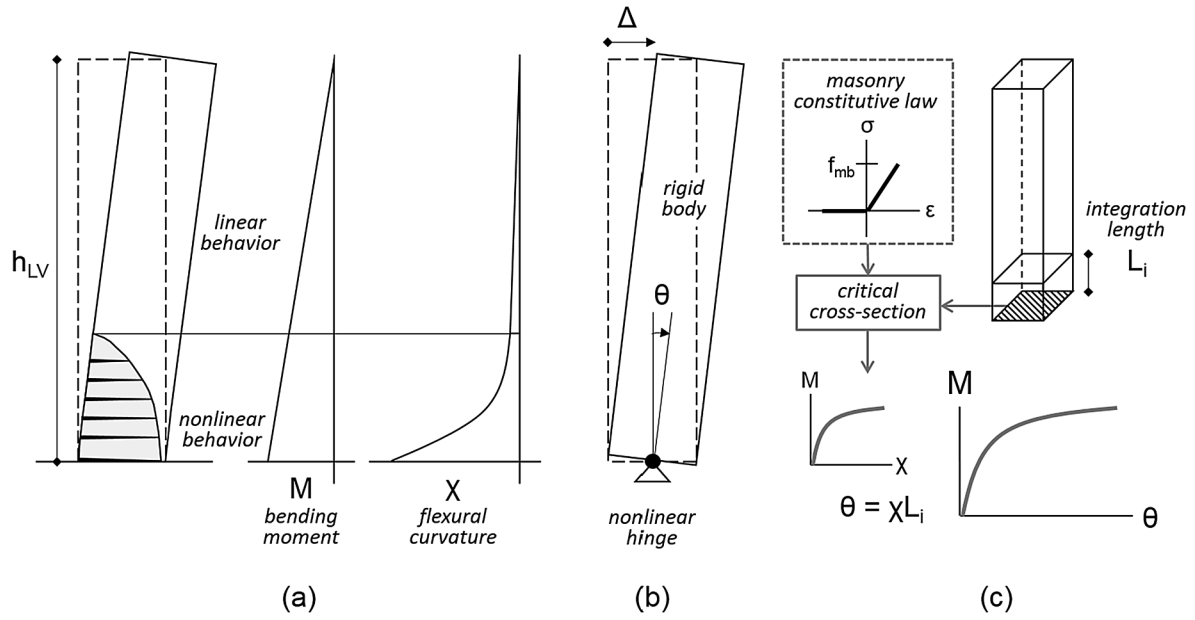

Fig. 4. Mechanical-based model: (a) OOP flexural response of the wall; (b) proposed mechanical-based model; (c) nonlinear hinge moment-rotation relationship definition.

$$M = \begin{cases} \frac{1}{12} E_m B t^3 \chi, & \chi \le \chi_{cr} \\ \bar{N}\left(\frac{t}{2} - \sqrt{\frac{2\bar{N}}{9 E_m B \chi}}\right), & \chi_{cr} \le \chi \le \chi_{lim} \end{cases} \quad (9)$$

where: $\bar{N}$ is the cross-section axial load which is equal to *(W + N)* for the cantilever case and *(W + N/2)* for the pinned-pinned and clamped-clamped cases; $\chi_{cr} = 2\bar{N}/(E_m B t^2)$ is the curvature at cracking limit; $\chi_{lim} = f_{mb}^2 B/(2E_m \bar{N})$ is the curvature at the achievement of the compressive limit of the material f_{mb}. Assuming that the curvature distribution over the integration length L_i is constant, the moment-rotation relationship of the nonlinear hinge is obtained multiplying the critical cross-section curvatures by L_i:

$$\theta = \chi \cdot L_i \quad (10)$$

Consequently, the top-wall OOP displacement Δ is proportional to the rotation θ (Fig. 4b):

$$\Delta = \theta \cdot h_{LV} \quad (11)$$

From Eqs. (10) and (11), the cross-section curvature is expressed as a function of the top displacement:

$$\chi = \frac{\Delta}{L_i h_{LV}} \quad (12)$$

Finally, imposing the rotational equilibrium of the wall around the nonlinear hinge and using Eqs. (10) and (11), the force displacement relation is derived. In the following the equations related to the three boundary conditions are reported. It can be observed that the equations are indirectly dependent from the compressive strength of the units f_{mb} through the curvature at limit, χ_{lim}.

Cantilever

$$F = \frac{1}{h_{LV}\alpha_h}\left(M - \frac{W\Delta}{2} - N\Delta\right)$$

for $\Delta \le L_i h_{LV} \chi_{cr}$:

$$F = \frac{1}{h_{LV}\alpha_h}\left(\frac{1}{12} E_m B t^3 \frac{\Delta}{L_i h_{LV}} - \frac{W\Delta}{2} - N\Delta\right)$$

for $L_i h_{LV} \chi_{cr} \le \Delta \le L_i h_{LV} \chi_{lim}$:

$$F = \frac{1}{h_{LV}\alpha_h}\left[(N + W)\left(\frac{t}{2} - \sqrt{\frac{2L_i t(N+W)}{9 E_m B \Delta}}\right) - \frac{W\Delta}{2} - N\Delta\right] \quad (13)$$

Pinned-Pinned

$$F = \frac{2}{h_{LV}\alpha_h}\left(M - \frac{W\Delta}{2} - N\Delta\right)$$

for $\Delta \le L_i h_{LV} \chi_{cr}$:

$$F = \frac{2}{h_{LV}\alpha_h}\left(\frac{1}{12} E_m B t^3 \frac{\Delta}{L_i h_{LV}} - \frac{W\Delta}{2} - N\Delta\right)$$

for $L_i h_{LV} \chi_{cr} \le \Delta \le L_i h_{LV} \chi_{lim}$:

$$F = \frac{2}{h_{LV}\alpha_h}\left[\left(N + \frac{W}{2}\right)\left(\frac{t}{2} - \sqrt{\frac{2L_i t(N + W/2)}{9 E_m B \Delta}}\right) - \frac{W\Delta}{2} - N\Delta\right] \quad (14)$$

Clamped-Clamped

$$F = \frac{2}{h_{LV}\alpha_h}\left(M - \frac{W\Delta}{4} - \frac{N\Delta}{2}\right)$$

for $\Delta \le L_i h_{LV} \chi_{cr}$:

$$F = \frac{2}{h_{LV}\alpha_h}\left(\frac{1}{12} E_m B t^3 \frac{\Delta}{L_i h_{LV}} - \frac{W\Delta}{4} - \frac{N\Delta}{2}\right)$$

for $L_i h_{LV} \chi_{cr} \le \Delta \le L_i h_{LV} \chi_{lim}$:

$$F = \frac{2}{h_{LV}\alpha_h}\left[\left(N + \frac{W}{2}\right)\left(\frac{t}{2} - \sqrt{\frac{4L_i t(N + W/2)}{9 E_m B \Delta}}\right) - \frac{W\Delta}{4} - \frac{N\Delta}{2}\right] \quad (15)$$

3. Numerical-experimental validation of the out-of-plane closed-form model

In order to validate the mechanical-based closed-form model described in Section 2.2, a review of the available OOP experimental tests on masonry walls has been conducted [25,31–33,43,44]. Among these, only static and pseudo-static tests have been considered. Additionally, experimental tests on cavity walls have not been considered since they are not representative of the construction practice in Nepal [9]. The result is a sample of seventeen OOP loading tests conducted for different geometries, masonry typologies, material properties, boundary conditions and applied vertical loads. Table 1 summarizes the main data, properties and sources of these tests. The *F-Δ* curves provided in these studies have been digitalized and postprocessed in order to obtain diagrams with uniform scale, where the total acting force *F* is plotted on the vertical axis and the maximum OOP displacement *Δ* on the horizontal one. Subsequently, all the tests have been compared with the four analytical models discussed in Section 2: *Bilinear* (Section 2.1.1), *Trilinear* (Section 2.1.2), *Quadrilinear* (Section 2.1.3), and the one proposed in this study and discussed in Section 2.2 (i.e., *Present study*).

Table 1
OOP experimental database.

#	Test name	Material				Geometry			B.C.*	Vertical load N [kN]	Horizontal force type	Authors	Ref.
		URM type	E_m [MPa]	f_{mb} [MPa]	γ_m [kN/m^3]	t [m]	B [m]	h [m]					
1	OP_PA1	Stone	490	43.83	21	0.65	1.30	2.50	C	0.0	Airbag	Ferreira et al. 2015	[33]
2	OP_PA2	Stone	490	43.83	21	0.65	1.30	2.50	C	52.0	Airbag	Ferreira et al. 2015	[33]
3	OP_PA3	Stone	490	43.83	21	0.65	1.30	2.50	C	140.0	Airbag	Ferreira et al. 2015	[33]
4	OP_PF1	Stone	490	43.83	21	0.65	1.30	2.50	C	0.0	Point Force	Ferreira et al. 2015	[33]
5	OP_PF2	Stone	490	43.83	21	0.65	1.30	2.50	C	52.0	Point Force	Ferreira et al. 2015	[33]
6	OP_PF3	Stone	490	43.83	21	0.65	1.30	2.50	C	140.0	Point Force	Ferreira et al. 2015	[33]
7	P_1	Rubble	1079	9.00[(a)]	19[(b)]	0.45	1.65	2.25	C	0.0	Point Force	Lagomarsino 2015	[25]
8	Panel_1	Rubble	690[(b)]	50.00	22	0.22	0.90	1.10	C	0.0	Point Force	Degli Abbiati et al. 2017	[31]
9	Panel_2	Rubble	690[(b)]	50.00	22	0.30	0.90	0.90	C	0.0	Point Force	Degli Abbiati et al. 2017	[31]
10	Panel_3	Rubble	690[(b)]	50.00	22	0.30	0.90	1.50	C	0.0	Point Force	Degli Abbiati et al. 2017	[31]
11	S_11	Brick	48[(c)]	14.2[(d)]	18	0.11	0.95	1.50	C-C	0	Point Force	Griffith et al. 2004	[32]
12	S_12	Brick	43[(c)]	15.7[(d)]	18	0.11	0.95	1.50	C-C	0	Point Force	Griffith et al. 2004	[32]
13	S_13	Brick	5[(c)]	15.7[(d)]	18	0.11	0.95	1.50	C-C	0	Point Force	Griffith et al. 2004	[32]
14	S_10	Brick	18[(c)]	26.7[(d)]	23	0.05	0.95	1.50	C-C	0	Point Force	Griffith et al. 2004	[32]
15	S_14	Brick	46[(c)]	26.3[(d)]	23	0.05	0.95	1.50	C-C	0	Point Force	Griffith et al. 2004	[32]
16	S_10L	Brick	710[(c)]	26.7[(d)]	23	0.05	0.95	1.50	C-C	3.55	Point Force	Griffith et al. 2004	[32]
17	S_14L	Brick	440[(c)]	26.3[(d)]	23	0.05	0.95	1.50	C-C	7.12	Point Force	Griffith et al. 2004	[32]

* Boundary Conditions: C = cantilever; P-P = pinned-pinned; C-C = clamped-clamped.
[(a)] In absence of specific experimental data, compressive strength of masonry units is assumed as three times the one of the masonry continuum (Eurocode 6 [45]).
[(b)] Data not reported in the source paper, therefore Italian Building Code indications are considered [46].
[(c)] Flexural elastic modulus estimated by Godio et al. [23] from the experimental tests by Griffith et al. [32].
[(d)] The source paper does not provide the compressive strength of the blocks f_{mb}. Conservatively, the compressive strength of the masonry continuum is adopted.

3.1. Description of the tests and comparison with analytical models

3.1.1. Ferreira et al. (2015)

The experimental campaign by Ferreira et al. [33] consists of six OOP loading tests on stone masonry walls. Three of these walls were tested by applying with a hydraulic jack a concentrated horizontal force at the top of the wall, while the other three were loaded with a pressure distribution generated through an airbag. The mechanical and geometrical characteristics of the six specimens are reported in Table 1 (from #1 to #6). The experimental campaign investigated three levels of vertical load *N*.

Figs. 5 and 6 report respectively the graphical comparison of one airbag test and one point-load test. Fig. 5a shows the comparison between the *F-Δ* curve of OP_PA3 (#3 referring to Table 1) and the curves obtained with the four analytical methods. In Fig. 5b, the relative error percentages with respect to the experimental results are evaluated for the four analytical models and plotted against the displacement (*Δ*) normalized with respect to the maximum experimental displacement ($\Delta_{max,exp}$). Furthermore, for each analytical model, the average value of the absolute error, $\mu(|e|)$, is reported. Analogous results are reported in Fig. 6 for test OP_PF1 (#4).

3.1.2. Lagomarsino (2015)

The test results reported in Lagomarsino [25] are related to a single pull-release OOP in a field experimental test conducted on one external wall of an existing masonry building located in Southern Italy. In this case, the load was applied through a cable equipped with an actuator. In Fig. 7a the numerical and experimental *F-Δ* diagrams are reported while in Fig. 7b the corresponding relative errors are shown.

3.1.3. Degli Abbiati et al. (2017)

Experimental tests by Degli Abbiati et al. [31] were performed for three stone masonry wallets by applying a concentrated force at 2/3 of the total height of the walls. The load was applied in quasi-static displacement-controlled conditions. Fig. 8 reports the results in terms of *F-Δ* curves and relative error for the first test (Panel_1, #8 in Table 1). It is noted that the experimental curve reported here is the maximum envelope of the one reported in [31].

3.1.4. Griffith et al. (2004)

The laboratory test from Griffith et al. [32] were performed with clamped-clamped boundary conditions. Fig. 9 reports the results for the test S_13 (#13 in Table 1). For these tests the quadrilinear methodology cannot be implemented since it does not fit for clamped-clamped boundaries.

3.2. Discussion of the results

Tables 2 and 3 summarize the mean value of the absolute errors $\mu(|e|)$ and the absolute error at experimental peak force $|e(\Delta_{peak,exp})|$ for cantilever configuration tests (#1 to #10) and clamped-clamped tests (#11 to #17) respectively. The first statistic $\mu(|e|)$ expresses the averaged predictive performance of a given analytical method with respect to the entire *F-Δ* experimental curve. The second quantity $|e(\Delta_{peak,exp})|$ indicates the model accuracy in estimating the lateral capacity at experimental peak force. Referring to cantilever tests, the average of $\mu(|e|)$ is 13.19% for the proposed formulation while it exceeds 20% for the multilinear models. Moreover, the mean of $|e(\Delta_{peak,exp})|$ is around 9% for novel/quadrilinear models and larger than 12% for bilinear/trilinear. The comparison with clamped-clamped tests shows larger errors for all the models. Therefore, the proposed approach leads to better predictions since the means of $\mu(|e|)$ and $|e(\Delta_{peak,exp})|$ have the smallest mismatch with experimental results (i.e., 31.17% and 11.49% respectively).

An additional comparison among the four analytical procedures can be done in terms of residual force at the maximum experimental displacement $\Delta_{max,exp}$. In this case the proposed model matches the test results with an average absolute error of 21% while for the other models the quantity exceeds 50%.

3.3. Evaluation of the optimum integration length L_i

As introduced in Section 2.2., the proposed closed-form mechanical model is based on the definition of the integration length L_i which is a challenging aspect for masonry structures [47]. In the present work L_i is expressed as a percentage of the shear length h_{LV}. In order to evaluate the optimum value of L_i, the experimental versus numerical comparisons described in Section 3.2. have been repeated for twelve values of L_i (ranging from $0.05 \cdot h_{LV}$ to $0.6 \cdot h_{LV}$). Fig. 10 reports the average error of

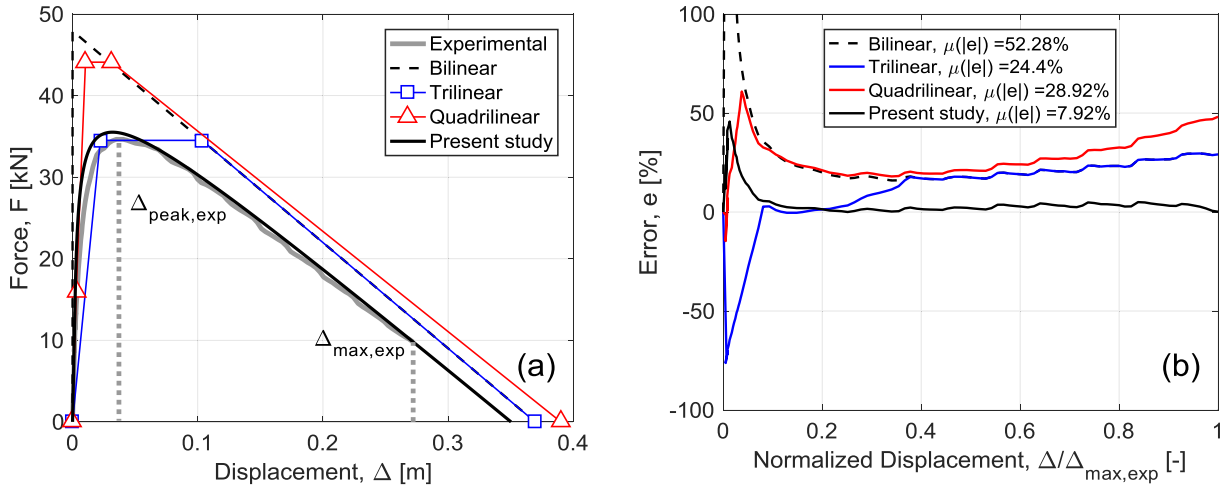

Fig. 5. Airbag OOP tests by Ferreira et al. [33] (#3 in Table 1): (a) *F-Δ* curves comparison; (b) error of the models with respect to the experimental curve.

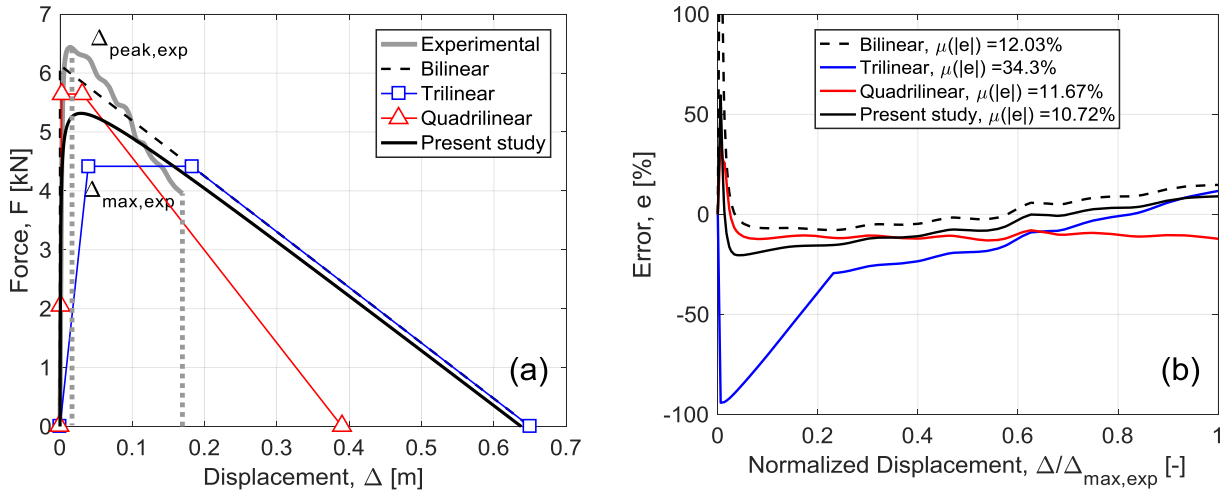

Fig. 6. Point force OOP tests by Ferreira et al. [33] (#4 in Table 1): (a) *F-Δ* curves comparison; (b) error of the models with respect to the experimental curve.

the proposed model with respect the 17 experimental tests in terms of $\mu(|e|)$ and $|e(\Delta_{peak,exp})|$, as defined in Section 3.2. It can be observed that the average error attains its minimum for integration length coefficients equal to *0.35* in terms of $\mu(|e|)$ and *0.15* in terms of $|e(\Delta_{peak,exp})|$, respectively. As a consequence of these results, an intermediate value of $0.25 \cdot h_{LV}$ has been selected for the model. It is important to underline that the present experimental calibration should be considered valid in the thickness (t) and vertical stress (σ_V) ranges of the experimental tests

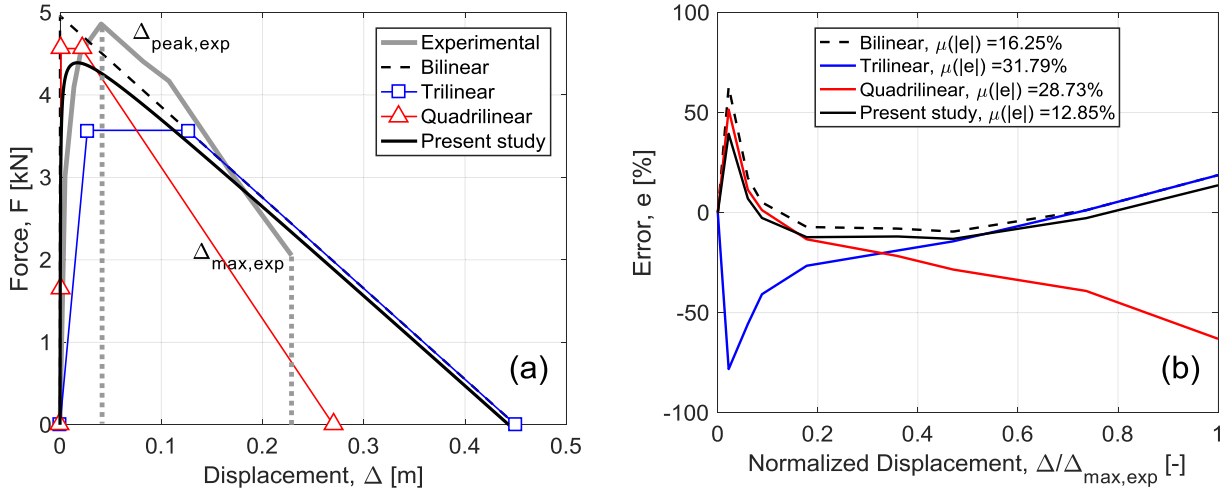

Fig. 7. Point load OOP in-field test reported by Lagomarsino [25] (#7 in Table 1): (a) *F-Δ* curves comparison; (b) error of the models with respect to the experimental curve.

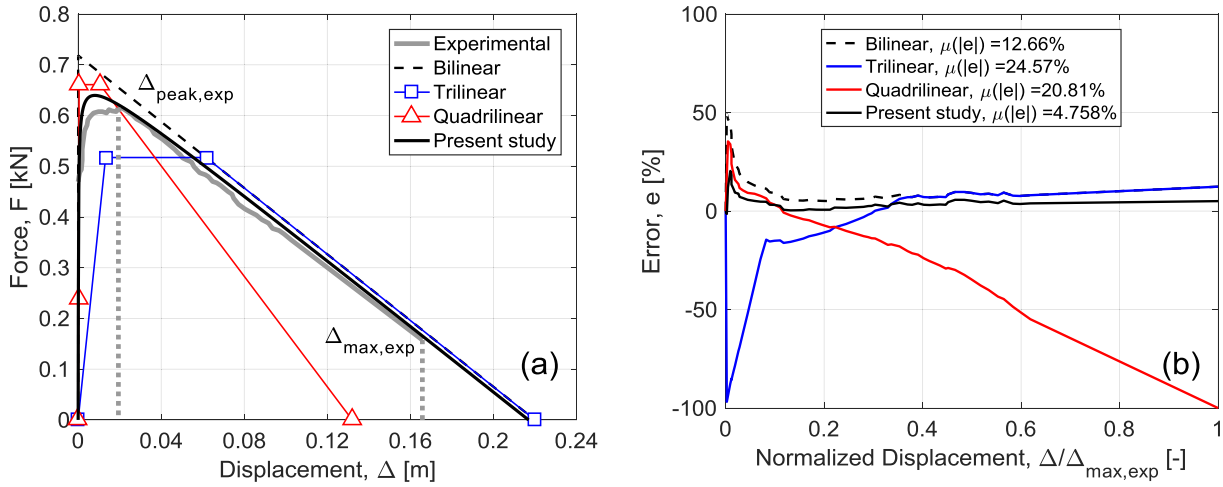

Fig. 8. OOP tests by Degli Abbiati et al. [31] (#8 in Table 1): (a) *F-Δ* curves comparison; (b) error of the models with respect to the experimental curve.

i.e.: (i) t between 5 cm and 65 cm; (ii) σ_V ranging from 0 MPa to 0.165 MPa.

4. Out-of-plane vulnerability assessment of a typical nepalese URM school building

The seismic vulnerability of a structure consists in its predisposition to be damaged when subjected to a specific level of seismic input. Consequently, as discussed by Calvi et al. [48], the goal of the vulnerability assessment is to estimate the intensity of the earthquake which generates a specific Damage State (DS) in the building. This intensity is usually expressed by a representative parameter of the ground shaking (i.e. the Intensity Measure IM) such as the Peak Ground Acceleration (PGA). Referring to the OOP vulnerability assessment of masonry buildings, IMs for corresponding DSs are usually calculated by adopting specific spectral-based approaches currently included in national codes and technical guidelines [46,49,50]. In general, spectral-based approaches assume that the OOP capacity of the building (or of a portion of the building) can be expressed in the form of a nonlinear-static *pushover* curve of an equivalent nonlinear Single-Degree-Of-Freedom (SDOF) system [24,25,34]. Subsequently, the IM corresponding to the OOP displacement of the considered DS are calculated in two ways.

One option is to estimate it through the displacement-based analysis methodology (as proposed in [24,51]). An elastic SDOF 'substitute structure' is defined so that achieves the same displacement of the real nonlinear SDOF system given a seismic excitation. Once the effective stiffness of the 'substitute structure' is defined, the IM corresponds to the spectral displacement which equates the DS displacement at the natural frequency of the 'substitute structure'.

The second option is to employ the CSM, originally developed by Freeman [52] and subsequently applied to the case of URM [25,30]. The *F-Δ* curve of the structure is reported in a spectral-displacement (S_d) vs. spectral-acceleration (S_a) plane. Then, the IM corresponding to the DS displacement is estimated by properly intersecting the *pushover* curve with the Acceleration Displacement Response Spectrum (ADRS) shape of the site. This intersection is performed by considering an equivalent damping coefficient which accounts for the energy dissipation of the system [49].

The use of spectral-based approaches for the OOP vulnerability assessment of masonry structures has been matter of debate in the last decades. For instance, Makris and Konstantinidis [53] have criticized the reliability of the equivalent SDOF idealization for the case of rocking structures. Instead, they have proposed a novel rocking response spectrum. However, as pointed out by Lagomarsino [25], this methodology is hardly applicable for the assessment of existing masonry structures since rocking spectra resulting from the Probabilistic Seismic Hazard Analyses (PSHA) are not yet available. Numerous scientific discussions have also been presented regarding the definition and selection of representative IMs for the OOP response of systems [54]. For instance, Dimitrakopoulos and Paraskeva [55] have pointed out that the overturning of rocking elements is poorly correlated with

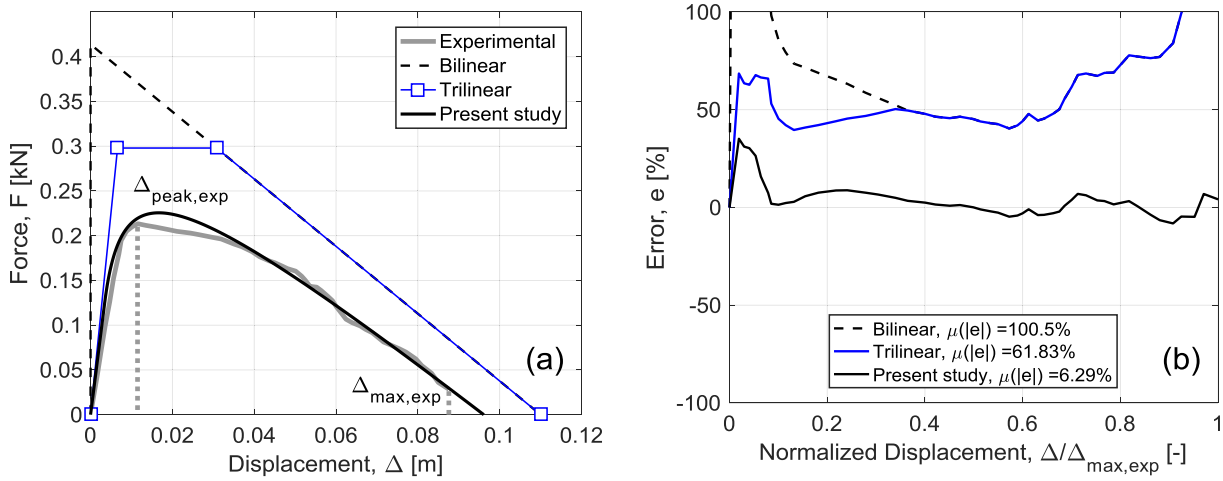

Fig. 9. OOP tests by Griffith et al. [32] (#13 in Table 1): (a) *F-Δ* curves comparison; (b) error of the models with respect to the experimental curve.

Table 2
Errors of the analytical solutions with respect to experimental tests (cantilever configuration).

#	μ(|e|) [%]				|e($\Delta_{peak,exp}$)| [%]			
	Bilinear	Trilinear	Quadrilinear	Present study	Bilinear	Trilinear	Quadrilinear	Present study
1	10.15	24.65	8.22	7.35	8.08	22.19	0.57	6.35
2	27.66	28.64	15.75	9.44	21.11	12.80	11.42	3.07
3	52.28	24.40	28.92	7.92	38.37	0.38	27.30	2.52
4	12.03	34.30	11.67	10.72	4.72	31.40	12.34	17.43
5	9.16	24.84	7.16	13.98	4.98	31.58	12.58	23.94
6	25.66	21.14	4.48	16.57	5.42	24.10	3.01	21.89
7	16.25	31.79	28.73	12.85	2.03	26.54	6.13	9.69
8	12.66	24.57	20.81	4.76	16.44	16.17	7.12	3.68
9	21.06	22.36	50.38	12.57	4.39	24.84	3.96	3.22
10	48.96	37.36	54.55	35.71	15.11	17.12	5.90	1.12
Average	23.59	27.40	23.07	13.19	12.06	20.71	9.03	9.29

Table 3
Errors of the analytical solutions with respect to experimental tests (clamped–clamped configuration).

#	μ(|e|) [%]			|e($\Delta_{peak,exp}$)| [%]		
	Bilinear	Trilinear	Present study	Bilinear	Trilinear	Present study
11	40.14	23.57	9.12	19.53	13.94	9.54
12	12.81	21.38	9.55	6.54	23.29	17.12
13	100.52	61.83	6.29	93.92	39.62	5.71
14	79.10	64.93	40.17	17.22	15.60	12.32
15	165.42	127.59	46.46	52.55	9.83	8.24
16	160.87	143.72	69.10	16.61	16.04	16.00
17	132.76	83.41	37.50	47.56	6.24	11.50
Average	98.80	75.20	31.17	36.27	17.80	11.49

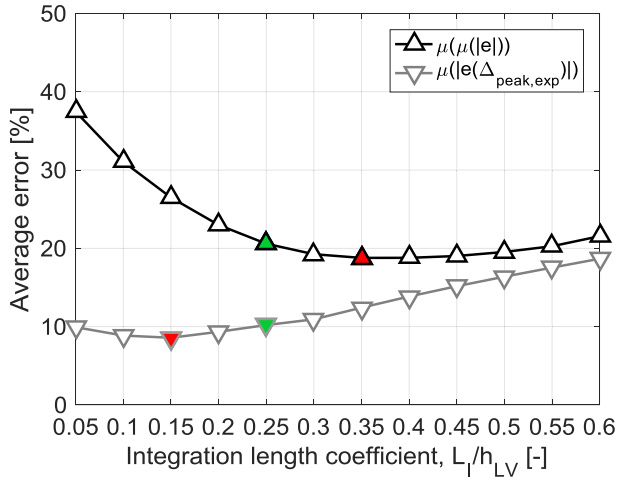

Fig. 10. Calibration of the integration length L_i by minimizing the error with respect to the experimental tests.

the PGA and depends primarily on the velocity characteristics of the ground motion. However, a recent research work by Giresini et al. [56], focused on the OOP fragility assessment of masonry facades, has verified that the PGA remains one of the most relevant IMs to define the response of a URM wall in OOP motion.

Starting from these considerations, in the following, the analytical solution described in Section 2.2 and validated in Section 3 is adopted to perform a spectral-based vulnerability assessment for a representative URM Nepalese school building. The case study structure is readapted from NSET [9] and it is a two-story building made of brick-mud masonry with timber joists-planks flooring system and galvanized-iron roof. Fig. 11 reports the plan view of the ground (Fig. 11a) and first (Fig. 11b) floors and the schematic elevation views (Fig. 11c). The maximum in-plan dimensions are 7.0 m × 7.5 m while the total height of the structure is 5 m. The thickness of the wall is equal to 0.35 m. The characteristics of the masonry material are taken from experimental tests on the same masonry typology reported in [57]. Particularly, the following values are adopted: masonry elastic modulus E_m = 794 MPa, bricks compressive strength f_{mb} = 11.03 MPa, masonry unit weight γ_m = 17.68 kN/m^3. It is noted that, from a structural-seismic point of view, the case-study is consistent with most of the damaged masonry buildings surveyed during the post-earthquake reconnaissance missions (e.g. [3,4,10,11]). Particularly, it is characterized by: (i) absence of adequate wall-to-wall and wall-to-floor connections; (ii) presence of flexible floor/roof; (iii) lack of seismic detailing. As already mentioned, under these conditions the walls of the structure behave independently, and the OOP failure is dominant.

The vulnerability assessment procedure presented herein consists in a three steps analysis: (1) walls classification; (2) *F-Δ* curves calculation and DSs definition; (3) estimation of IMs for the corresponding DSs. PGA is chosen as the IM for this study.

4.1. Walls classification

To perform the OOP vulnerability assessment of a masonry building it is important to consider all the possible collapse mechanism which are likely to happen during a seismic event (e.g. D'Ayala and Speranza [34]). Accordingly, the first assessment step consists of identifying the vulnerable walls. Given the structural deficiencies of URM Nepalese buildings [1,10,12], any of the vertically disconnected walls is herein considered as vulnerable. A classification of the walls with respect to their boundary conditions and overburden load is therefore needed. Referring to Fig. 11:

- The walls labelled as C (blue-crossed) are non-loadbearing. As in Doherty et al. [24], they are characterized by cantilever boundary configuration and absence of vertical overloads. Additionally, since they are not connected to the floor beams (which is typical in Nepalese URMs [10]), their vertical span is equal to 5 m (i.e., total height of the building).
- The walls labelled as C-C_{GF} (green-dotted) are located at the ground floor and according to [24] are characterized by clamped-clamped boundary condition. Their vertical load is the sum of the load transferred from the first floor, the overload of the roof and the self-weight of the second-story walls. The vertical span of these walls is equal to 2.4 m.
- The walls labelled as C_{FF} (red-dashed), located at the first floor, support the weight of the roof and are assumed with cantilever boundary configuration. As a matter of fact the light galvanized-iron paneled roof is generally disconnected to the walls and, therefore, is not able to restrain OOP displacements (as shown in some of the

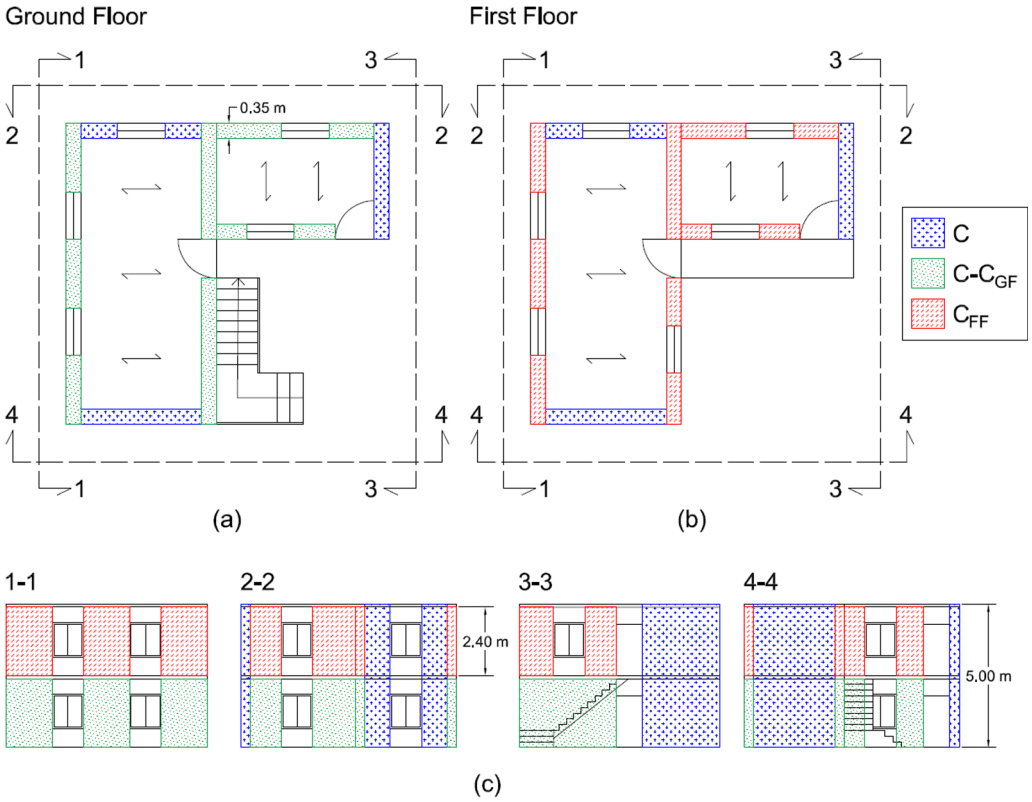

Fig. 11. Case-study URM Nepalese school building: (a) plan view of the ground floor; (b) plan view of the first floor; (c) elevation views.

photographic documentation reported in EERI [4]).

According to the information provided in [9,57], the floor overload is quantified considering the wooden structure (timber joists plus planks, equal to 0.5 kN/m^2) and a 10 cm thick mud-layer (1.7 kN/m). The galvanized-iron sheeting roof is assumed 0.2 kN/m^2 according to the Indian Standards IS 875 [58] (reference document for the Nepalese Building Code (NBC) [59]). A fraction of 30% of the code compliant live load is also taken into account (0.3 × 3.0 kN/m^2 = 0.9 kN/m^2 [58,60]). Table 4 summarizes the wall classification.

4.2. Force-displacement curve calculation and DS definition

Fig. 12a reports the *F-Δ* curves of the three different walls configurations considering a representative width B = 1 m. As expected, the non-loadbearing walls (configuration C) and the ones at upper stories (configuration C_{FF}) are characterized by lower transversal force capacity. From the *F-Δ* curve, the damage thresholds are directly calculated in accordance with spectral procedures available in literature (e.g. Lagomarsino [25] and Rota et al. [61]). Herein, the following damage limit states are considered:

- DS1 (slight damage) corresponds to the displacement at the attainment of 70% of the peak horizontal force;
- DS2 (moderate damage) is defined at the peak displacement Δ_{peak};
- DS3 (severe damage) is assumed at 25% of the ultimate displacement (i.e., displacement corresponding to null force);
- DS4 (near collapse) corresponds to 40% of the ultimate displacement.

The described damage states are shown on the $S_a - S_d$ plane in Fig. 12b for configuration C.

4.3. IM estimation for corresponding DS

To evaluate the IM correspondent to a specific DS, an appropriate capacity-demand procedure has to be implemented. As previously mentioned, the CSM [52] is adopted for the case. Differently from the N2 Method [62], which is based on the concept of ductility and behavior factor, the CSM relies on the definition of an equivalent damping coefficient. For the specific case of OOP vulnerability assessment of masonry structures, Lagomarsino [25] has extensively discussed and validated the suitability of CSM with respect to the other techniques. The first step of the CSM is to transform the *F-Δ* curve in a capacity curve defined in a spectral-acceleration (S_a) versus spectral-displacement (S_d) plane. As in Doherty et al. [24], the transformation is performed with the following equations:

Table 4
Walls classification.

Configuration	Boundary condition*	Floor location	Height H [m]	**Overburden N [kN]** **
C	Cantilever	Ground + First	5.0	0
C-C$_{GF}$	Clamped-clamped	Ground	2.4	20.1
C$_{FF}$	Cantilever	First	2.4	0.3

* Refer to Fig. 2.
** The overburden N is calculated for a unitary width B = 1 m.

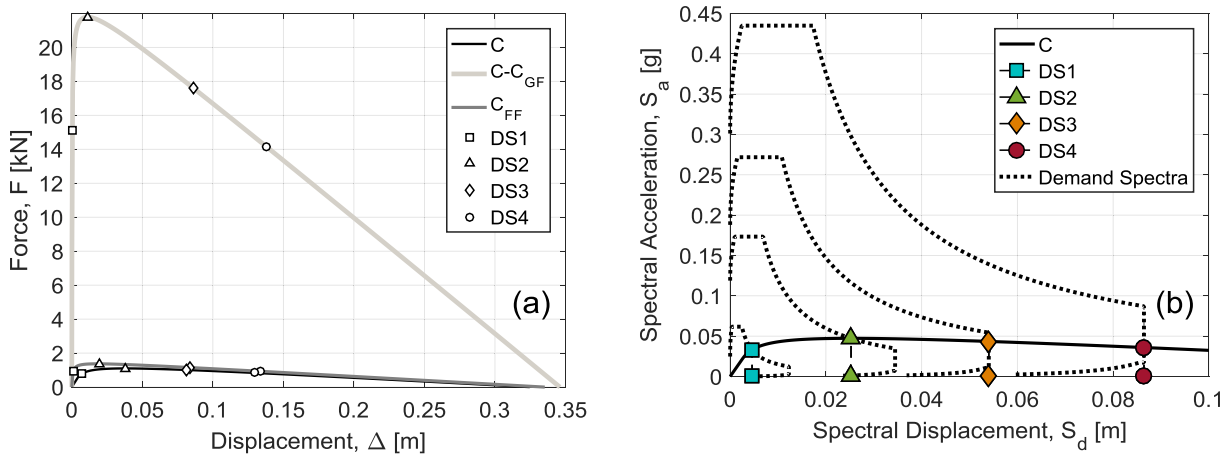

Fig. 12. (a) *F-Δ* curves; (b) capacity vs demand assessment for configuration C.

$$\begin{cases} S_a = \frac{F}{M_e};\ M_e = \frac{(\sum_{i=1}^{n} m_i \delta_i)^2}{\sum_{i=1}^{n} m_i \delta_i^2} \\ S_d = \Delta \cdot \Delta_e;\ \Delta_e = \frac{\sum_{i=1}^{n} m_i \delta_i^2}{\sum_{i=1}^{n} m_i \delta_i} \end{cases} \quad (16)$$

where: M_e is the effective mass of the equivalent SDOF system estimated by discretizing the wall into a finite number of elements with mass m_i and modal displacement δ_i; Δ_e is the effective displacement of the SDOF. From Eq. (16), it can be noted that the capacity curve of the wall is independent from the width B. More specifically, since F and M_e are linearly proportional with B, S_a depends only on the wall configuration (Table 3). Furthermore, Δ_e is independent from B and so is the spectral displacement S_d. From the DS defined on the capacity curve, the corresponding periods T_{DS} are estimated as:

$$T_{DS} = 2\pi \sqrt{\frac{S_{d,DS}}{S_{a,DS}}} \quad (17)$$

and the equivalent damping coefficients ξ_{DS} for any DS [35] become:

$$\xi_{DS} = \xi_0 + \xi_{h,MAX}\left(1 - \frac{1}{\mu_{DS}^{\zeta}}\right) \quad (18)$$

where, according to Lagomarsino et al. [35], ξ_0 is the initial damping of the structure which ranges from 3% to 5%, $\xi_{h,MAX}$ is the asymptote of the hysteretic damping which depends on the type of structure (Table 5) and μ_{DS}^{ζ} is the displacement ductility defined as Δ_{DS}/Δ_{DS1} with exponent ζ ranging from 1 and 2.

Considering the nature of the problem, from Table 5 it results that $\xi_{h,MAX}$ = 20% (Type B) is the value to adopt for the OOP assessment of masonry building without box behavior and therefore subjected to OOP damage. However, since the definition of a correct $\xi_{h,MAX}$ is fundamental for a proper implementation of the CSM and it affects the final PGA capacity, in Section 4.3.1. This value is calibrated with respect to experimental shaking-table test results by Al Shawa et al. [27].

The final step of the assessment procedure is the calculation of the IM for each DS. A normalized ADRS demand spectrum (PGA = 1.0 g) is constructed. Since the Nepalese Building Code [59] does not provide elastic response spectrum equations (i.e., it provides only the inelastic design spectra similarly to some pre-1990 codes such as the Italian DM3/3/1975 [63]), the spectral shape of the Eurocode 8 [64] is used. In particular, the spectral shape for Type I and soil A is adopted. Lastly, the IM is estimated by scaling the normalized ADRS in order to intersect the capacity curve at the given DS [25,35]. It is underlined that, for the walls located at the upper floors, specific amplified response spectra have to be considered [65,66]. In the present study the equations proposed by Lagomarsino [25] are adopted. For any DS, the lowest PGA from the different wall configurations is representative of the entire building. Fig. 12b reports the capacity versus demand assessment conducted for the walls in configuration C.

4.3.1. Calibration of $\xi_{h,MAX}$ with respect to shaking table tests by al Shawa et al. (2012)

The experimental campaign by Al Shawa et al. [27] consists of 34 one-component shaking table tests of one simple masonry structure composed by the façade (located perpendicularly with respect to the seismic action) and two transverse walls, resulting in an overall U-plan configuration. Despite the experimental tests were carried out for the assessment of masonry structures in Mediterranean countries, the masonry typology could be representative of Nepalese URMs since there is no interlocking between orthogonal walls (i.e. façade and transversal panels) and the frontal wall is able to deform in the OOP direction without any restraint. The geometrical characteristics of the structure are: length of 3.3 m for the façade and 2.3 m for the transversal walls; height of the specimen 3.44 m; thickness 0.25 m. The mechanical characteristics of the masonry material are: elastic modulus E_m = 1080 MPa (from the Italian Building Code [46]); compressive strength of units f_{mb} = 5.98 MPa. The 34 shaking table tests were performed considering three ground motion from the 1980 Irpinia (Italy) earthquake and one record from the 1997 Umbria-Marche (Italy) earthquake (response spectra reported in Fig. 13b) with different scale factors. More details of the experimental tests are reported in the source paper [27].

The calibration of $\xi_{h,MAX}$ is executed by considering five possible values, from 5% to 25%. For any of these values, the following steps are carried out:

i. estimation of the capacity curve of the façade adopting the closed-

Table 5
Values of $\xi_{h,MAX}$ for different type of structures (from [35]).

Type	A Structures with box-behavior	B Structure analyzable by independent macro-elements	C Assets characterized by one-dimensional masonry elements	D Arched structures subject to in-plane damage	F Blocky structures subjected to overturning
$\xi_{h,MAX}$	25	20	15	15	5

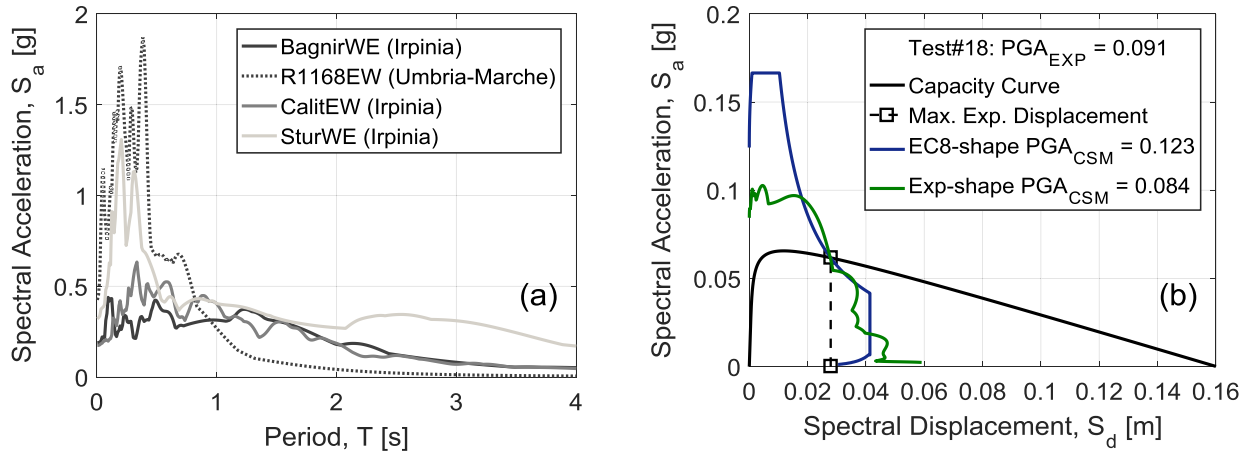

Fig. 13. (a) Response spectra of the ground motion records adopted in Al Shawa et al. [27]; (b) CSM implementation for EC8-shape and Exp-shape spectra.

form mechanical-based solution reported in Section 2.2. Representation of the experimental maximum displacement on the capacity curve;

ii. evaluation of the PGA that correspond to the attainment of the experimental maximum displacement through the CSM;

iii. calculation of the PGA_{EXP}/PGA_{CSM} ratio, where PGA_{EXP} refers to the experimental test while PGA_{CSM} is the one estimated from the spectral-based procedure;

iv. repetition of the procedure for the whole set of tests.

The CSM is herein executed either adopting the spectral shape of the Eurocode 8 [64] (EC8) and the spectral shape of the ground motion used for the test (Exp). The outcome of the procedure previously described is reported in Fig. 13b (Test #18 referring to the source paper numbering [27]). The black-solid line represents the OOP capacity curve of the wall; the black-square marker indicates the maximum experimental displacement; the blue and the green curves are the EC8-shape and Exp-shape spectra calculated with the CSM so that intersect the capacity curve at the experimental maximum displacement.

Lastly, in Fig. 14, the boxplot of the ratios PGA_{EXP}/PGA_{CSM} are reported for the different value of $\xi_{h,MAX}$ (values PGA_{EXP}/PGA_{CSM} greater than 1 lead to conservative assessment). It can be observed that in terms of median value the ground-motion spectral shape (Exp) gives always conservative estimation of the PGA with respect to the real value. Additionally, when considering the EC8 spectral shape, $\xi_{h,MAX}$=10% is the value which minimize the error at the median.

Table 6
Comparison between analytical assessment results and median PGA from observational fragility curves.

	Damage State	PGA	
		$\xi_{h,MAX}$ = 20% [35]	$\xi_{h,MAX}$ = 10%
Present Study	DS1	0.02	0.02
	DS2	0.12	0.10
	DS3	0.19	0.15
	DS4	0.30	0.24
Chaulagain et al.	Moderate	0.12	
	Extensive	0.19	
	Collapse	0.35	
Gautam et al.	DS-1	0.13	
	DS-2	0.16	
	DS-3	0.22	

4.4. Discussion of the assessment results

Table 6 reports the values of PGA for the four DS discussed in 4.2 by considering $\xi_{h,MAX}$ equal to 20% (following the recommendations of Lagomarsino and Cattari [35]) and to 10% (based on the calibration to experimental data in 4.3.1.). The quantities are compared with the median values of the observational fragility curves derived by Chaulagain et al. [67] and by Gautam et al. [68] for Nepalese unreinforced masonry buildings. It is specified that these works are based on the definition of three DS which correspond to DS2, DS3 and DS4 of the present study. There is a good agreement between analytical PGAs and median empirical values for both $\xi_{h,MAX}$ values. In general,

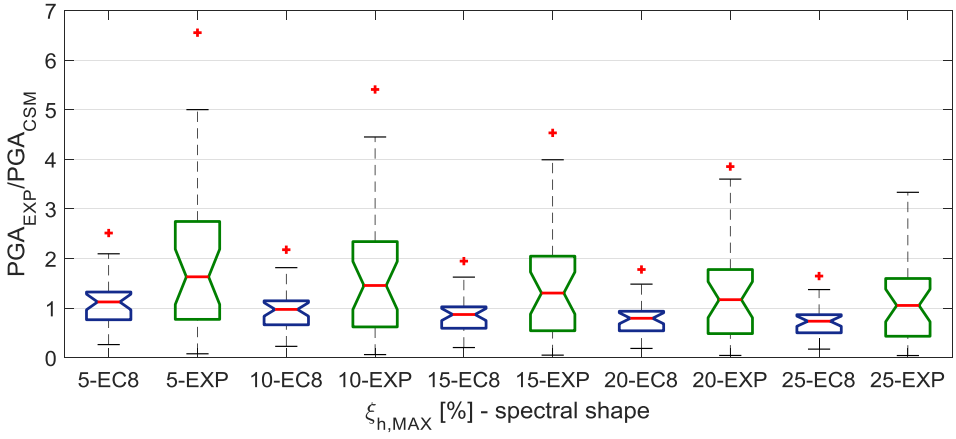

Fig. 14. Box plot for different $\xi_{h,MAX}$ and spectral shapes ranging from 5% to 25% evaluated for EC8 and experimental spectral shapes.

$\xi_{h,MAX}$ = 10% produces more conservative results. The PGA evaluated analytically for DS2 and $\xi_{h,MAX}$ = 10% is 0.10 g while the two empirical values are 0.12 g and 0.13 respectively. Similarly, the PGA estimation for DS3 is 0.15 g for the analytical procedure and at 0.19 g and 0.16 g for the Chaulagain et al. and Gautam et al.'s studies, respectively. Lastly, in DS4, the value of PGA is 0.24 g for the proposed methodology and 0.35 g, 0.22 g for the empirical benchmarks.

5. Conclusions

The vulnerability assessment of school buildings is a fundamental step for the implementation of effective risk mitigation policies in low-income countries such as Nepal. The present study proposes a novel mechanical-based closed-form solution for the OOP seismic assessment of these structures. The main conclusions of the work can be summarized as follows:

- The novel closed-form model has simulated the experimental F-Δ response of seventeen OOP tests with an average error of about 20% (10% when calculated at the peak experimental force). Furthermore, its predictive performance results better when compared with three closed-form piecewise linear models available in the literature [24,28,29].
- By adopting the proposed model, OOP vulnerability assessment of a typical Nepalese URM school building was carried out with the CSM. PGA values for different DSs are in very good agreement with the median values from empirical fragility curves of Nepalese buildings [67,68].
- Additionally, CSM asymptotic hysteretic equivalent damping $\xi_{h,MAX}$ has been calibrated with OOP experimental shaking table tests by Al Shawa et al. [27], providing a suggested value of 10%.

The assessment methodology presented is aimed to be straightforward and applicable at large scale without incurring in significant analysis costs (e.g. software purchase, implementation time, etc.). The approach, meant for school buildings in Nepal, can be extended to other URM building categories (e.g., residential, commercial, etc.) and used in other geographical locations where URMs are characterized by poor wall-to-wall and wall-to-floor connections, so that OOP damage is the dominant failure mode.

Acknowledgments

This work was funded by the UK Engineering and Physical Science Research Council (EPSRC) under the project "Seismic Safety and Resilience of Schools in Nepal" SAFER (EP/P028926/1), http://www.safernepal.net/. The underlying data for this study were drawn from the referenced literature. The full experimental versus analytical comparison is available for download from the Research Data Repository of University of Bristol at https://doi.org/10.5523/bris.27nzx9mu9uk382icl4qj1o8mmi.

References

[1] Gautam Dipendra, Chaulagain Hemchandra. Structural performance and associated lessons to be learned from world earthquakes in Nepal after 25 April 2015 (MW 7.8) Gorkha earthquake. Eng Fail Anal 2016;68:222–43. https://doi.org/10.1016/j.engfailanal.2016.06.002.
[2] Aon Benfield. 2015 Nepal earthquake event recap report. London, UK; 2015.
[3] Build change. April 25, 2015 – Gorkha earthquake, Nepal – post-disaster reconnaissance report. Denver, USA; 2015.
[4] EERI Earthquake Engineering Research Institute. M7.8 Gorkha, Nepal earthquake on April 25, 2015 and its aftershocks. Oakland, CA, USA; 2016.
[5] Government of Nepal. Nepal earthquake 2015 - post disaster needs assessment. Kathmandu, Nepal; 2015.
[6] Paci-Green R, Pandley B, Friedman R. Post-earthquake comparative assessment of school reconstruction and social impacts in Nepal. USA; 2015.
[7] Asian development bank. Strategy and plan for increasing disaster resilience for schools in Nepal. Bangkok, Thailand, Thailand; 2014.
[8] Chaulagain H, Rodrigues H, Jara J, Spacone E, Varum H. Seismic response of current RC buildings in Nepal: A comparative analysis of different design/construction. Eng Struct 2013;49:284–94. https://doi.org/10.1016/j.engstruct.2012.10.036.
[9] National Society for Earthquake Technology (NSET). Seismic vulnerability of the public school buildings of Kathmandu Valley and methods for reducing it. Kathmandu, Nepal; 2000.
[10] Gautam D, Rodrigues H, Bhetwal KK, Neupane P, Sanada Y. Common structural and construction deficiencies of Nepalese buildings. Innov Infrastruct Solut 2016;1:1. https://doi.org/10.1007/s41062-016-0001-3.
[11] Sharma K, Deng L, Noguez CC. Field investigation on the performance of building structures during the April 25, 2015, Gorkha earthquake in Nepal. Eng Struct 2016;121:61–74. https://doi.org/10.1016/j.engstruct.2016.04.043.
[12] Brando G, Rapone D, Spacone E, O'Banion MS, Olsen MJ, Barbosa AR, et al. Damage reconnaissance of unreinforced masonry bearing wall buildings after the 2015 Gorkha, Nepal, Earthquake. Earthq Spectra 2017;33:S243–73. https://doi.org/10.1193/010817EQS009M.
[13] de Felice G. Out-of-plane seismic capacity of masonry depending on wall section morphology. Int J Archit Herit 2011;5:466–82. https://doi.org/10.1080/15583058.2010.530339.
[14] Costa A. Structural rehabilitation of old buildings Netherlands: Springer; 2014. https://doi.org/10.1007/978-3-642-39686-1.
[15] Como M. Statics of historic masonry constructions. Netherlands: Springer; 2013.
[16] Laghi V, Palermo M, Trombetti T, Schildkamp M. Seismic-proof buildings in developing countries. Front Built Environ 2017;3:1–12. https://doi.org/10.3389/fbuil.2017.00049.
[17] Lourenço PB, Mendes N, Ramos LF, Oliveira DV. Analysis of masonry structures without box behavior. Int J Archit Herit 2011;5:369–82. https://doi.org/10.1080/15583058.2010.528824.
[18] Ferreira TM, Costa AA, Costa A. Analysis of the out-of-plane seismic behavior of unreinforced masonry: A literature review. Int J Archit Herit 2015;9:949–72. https://doi.org/10.1080/15583058.2014.885996.
[19] Lemos JV. Discrete element modeling of masonry structures. Int J Archit Herit 2007;1:190–213. https://doi.org/10.1080/15583050601176868.
[20] Silva LC, Lourenço PB, Milani G. Nonlinear discrete homogenized model for out-of-plane loaded masonry walls. J Struct Eng 2017;143:04017099. https://doi.org/10.1061/(ASCE)ST.1943-541X.0001831.
[21] La Mendola L, Papia M, Zingone G. Stability of masonry walls subjected to seismic transverse forces. J Struct Eng 1995;121:1581–7. https://doi.org/10.1061/(ASCE)0733-9445(1995) 121:11(1581).
[22] Cavaleri L, Fossetti M, Papia M. Modeling of out-of-plane behavior of masonry walls. J Struct Eng 2009;135:1522–32. https://doi.org/10.1061/(ASCE)0733-9445(2009) 135:12(1522).
[23] Godio M, Beyer K. Analytical model for the out-of-plane response of vertically spanning unreinforced masonry walls. Earthq Eng Struct Dyn 2017;46:2757–76. https://doi.org/10.1002/eqe.2929.
[24] Doherty K, Griffith MC, Lam N, Wilson J. Displacement-based seismic analysis for out-of-plane bending of unreinforced masonry walls. Earthq Eng Struct Dyn 2002;31:833–50. https://doi.org/10.1002/eqe.126.
[25] Lagomarsino S. Seismic assessment of rocking masonry structures. Bull Earthq Eng 2015;13:97–128. https://doi.org/10.1007/s10518-014-9609-x.
[26] De Felice G, Giannini R. Out-of-plane seismic resistance of masonry walls. J Earthq Eng 2001;5:253–71. https://doi.org/10.1080/13632460109350394.
[27] Al Shawa O, de Felice G, Mauro A, Sorrentino L. Out-of-plane seismic behaviour of rocking masonry walls. Earthq Eng Struct Dyn 2012;41:949–68. https://doi.org/10.1002/eqe.1168.
[28] Heyman J. The stone skeleton. Int J Solids Struct 1966;2:249–79. https://doi.org/10.1016/0020-7683(66)90018-7.
[29] Ferreira TM, Costa AA, Vicente R, Varum H. A simplified four-branch model for the analytical study of the out-of-plane performance of regular stone URM walls. Eng Struct 2015;83:140–53. https://doi.org/10.1016/j.engstruct.2014.10.048.
[30] D'Ayala DF, Paganoni S. Assessment and analysis of damage in L'Aquila historic city centre after 6th April 2009. Bull Earthq Eng 2011;9:81–104. https://doi.org/10.1007/s10518-010-9224-4.
[31] Degli Abbati S, Lagomarsino S. Out-of-plane static and dynamic response of masonry panels. Eng Struct 2017;150:803–20. https://doi.org/10.1016/j.engstruct.2017.07.070.
[32] Griffith MC, Lam NTK, Wilson JL, Doherty K. Experimental investigation of unreinforced brick masonry walls in flexure. J Struct Eng 2004;130:423–32. https://doi.org/10.1061/(ASCE)0733-9445(2004) 130:3(423).
[33] Ferreira TM, Costa AA, Arede A, Gomes A, Costa A. Experimental characterization of the out-of-plane performance of regular stone masonry walls, including test setups and axial load influence. Bull Earthq Eng 2015;13:2667–92. https://doi.org/10.1007/s10518-015-9742-1.
[34] D'Ayala D, Speranza E. Definition of collapse mechanisms and seismic vulnerability of historic masonry buildings. Earthq Spectra 2003;19:479–509. https://doi.org/10.1193/1.1599896.
[35] Lagomarsino S, Cattari S. PERPETUATE guidelines for seismic performance-based assessment of cultural heritage masonry structures. Bull Earthq Eng 2015;13:13–47. https://doi.org/10.1007/s10518-014-9674-1.
[36] Frisch-Fay R. Stability of masonry piers. Int J Solids Struct 1975;11:187–98. https://doi.org/10.1016/0020-7683(75)90052-9.
[37] Parisi F, Augenti N. Assessment of unreinforced masonry cross sections under eccentric compression accounting for strain softening. Constr Build Mater 2013;41:654–64. https://doi.org/10.1016/j.conbuildmat.2012.12.039.
[38] Parisi F, Sabella G, Augenti N. Constitutive model selection for unreinforced masonry cross sections based on best-fit analytical moment-curvature diagrams. Eng

Struct 2016;111:451–66. https://doi.org/10.1016/j.engstruct.2015.12.036.
[39] Brencich A, de Felice G. Brickwork under eccentric compression: Experimental results and macroscopic models. Constr Build Mater 2009;23:1935–46. https://doi.org/10.1016/j.conbuildmat.2008.09.004.
[40] Cavaleri L, Failla A, La Mendola L, Papia M. Experimental and analytical response of masonry elements under eccentric vertical loads. Eng Struct 2005;27:1175–84. https://doi.org/10.1016/j.engstruct.2005.02.012.
[41] Giordano N, Crespi P, Franchi A. Flexural strength-ductility assessment of unreinforced masonry cross-sections: analytical expressions. Eng Struct 2017;148:399–409. https://doi.org/10.1016/j.engstruct.2017.06.047.
[42] Crespi P, Franchi A, Giordano N, Scamardo M, Ronca P. Structural analysis of stone masonry columns of the Basilica S. Maria di Collemaggio. Eng Struct 2016;129:81–90. https://doi.org/10.1016/j.engstruct.2016.05.045.
[43] Graziotti F, Tomassetti U, Penna A, Magenes G. Out-of-plane shaking table tests on URM single leaf and cavity walls. Eng Struct 2016;125:455–70. https://doi.org/10.1016/j.engstruct.2016.07.011.
[44] Tomassetti U, Graziotti F, Penna A, Magenes G. Modelling one-way out-of-plane response of single-leaf and cavity walls. Eng Struct 2018;167:241–55. https://doi.org/10.1016/j.engstruct.2018.04.007.
[45] Comité Européen de Normalisation. EN 1996-1-1:2005. Eurocode 6: design of masonry structures – Part 1–1: General rules for reinforced and unreinforced masonry structures. Brussels; 2005.
[46] Ministero delle Infrastrutture e dei Trasporti. Circolare Esplicativa 2 febbraio 2009 n. 617. Rome, Italy; 2009.
[47] Fabbrocino F, Ramaglia G, Lignola GP, Prota A. Ductility-based incremental analysis of curved masonry structures. Eng Fail Anal 2019;97:653–75. https://doi.org/10.1016/j.engfailanal.2019.01.027.
[48] Calvi GM, Pinho R, Magenes G, Bommer JJ, Restrepo-Vélez LF, Crowley H. Development of seismic vulnerability assessment methodologies over the past 30 years. ISET J{…} 2006;43:75–104. https://doi.org/10.1109/JSTQE.2007.897175.
[49] American Society of Civil Engineers (ASCE). FEMA 356 prestandard and commentary for the seismic rehabilitation of building. Rehabilitation 2000.
[50] NZSEE. The seismic assessment of existing buildings - technical guidelines for engineering assessment; 2017.
[51] Griffith MC, Magenes G, Melis G, Picchi L. Evaluation of out-of-plane stability of unreinforced masonry walls subjected to seismic excitation. J Earthq Eng 2003;7:141–69. https://doi.org/10.1080/13632460309350476.
[52] Freeman SA. Review of the development of the capacity spectrum method. ISET J Earthq Technol 2004;41:113.
[53] Makris N, Konstantinidis D. The rocking spectrum and the limitations of practical design methodologies. Earthq Eng Struct Dyn 2003. https://doi.org/10.1002/eqe.223.
[54] Bachmann JA, Strand M, Vassiliou MF, Broccardo M, Stojadinović B. Is rocking motion predictable? Earthq Eng Struct Dyn 2018. https://doi.org/10.1002/eqe.2978.
[55] Dimitrakopoulos EG, Paraskeva TS. Dimensionless fragility curves for rocking response to near-fault excitations. Earthq Eng Struct Dyn 2015;44:2015–33. https://doi.org/10.1002/eqe.2571.
[56] Giresini L, Casapulla C, Denysiuk R, Matos J, Sassu M. Fragility curves for free and restrained rocking masonry façades in one-sided motion. Eng Struct 2018;164:195–213. https://doi.org/10.1016/j.engstruct.2018.03.003.
[57] Research center for disaster mitigation of urban cultural heritage. Disaster risk management for the Historic City of Patan, Nepal. Kyoto, Japan; 2012.
[58] Bureau of Indian Standards (BIS). IS 875: code of practice for design loads (other than earthquake) for buildings and structures. New Delhi, India; 1987.
[59] Department of urban development and building construction. Nepal national building code. Kathmandu, Nepal; 1994.
[60] Ministero delle Infrastrutture e dei Trasporti. NTC 2008 (Italian Building Code). Rome, Italy; 2008.
[61] Rota M, Penna A, Magenes G. A methodology for deriving analytical fragility curves for masonry buildings based on stochastic nonlinear analyses. Eng Struct 2010;32:1312–23. https://doi.org/10.1016/j.engstruct.2010.01.009.
[62] Fajfar P. Capacity spectrum method based on inelastic demand spectra. Earthq Eng Struct Dyn 1999;28:979–93. https://doi.org/10.1002/(SICI)1096-9845(199909)28:9<979::AID-EQE850>3.0.CO;2-1.
[63] Ministero delle Infrastrutture e dei Trasporti. DM3/3/1975 - Approvazione delle norme tecniche per le costruzioni in zone sismiche. Rome, Italy; 1975.
[64] European Commitee for Standardization. Eurocode 8: Design of structures for earthquake resistance - Part 1: General rules, seismic actions and rules for buildings. Eur Comm Stand 2004;1:231. [Authority: The European Union per Regulation 305/2011, Directive 98/34/EC, Directive 2004/18/EC].
[65] Suarez LE, Singh MP. Floor response spectra with structure-equipment interaction effects by a mode synthesis approach. Earthq Eng Struct Dyn 1987;15:141–58.
[66] Calvi PM, Sullivan TJ. Estimating floor spectra in multiple degree of freedom systems. Earthquakes Struct 2014;7(17–38). https://doi.org/10.12989/eas.2014.7.1.017.
[67] Chaulagain H, Rodrigues H, Silva V, Spacone E, Varum H. Earthquake loss estimation for the Kathmandu Valley. Bull Earthq Eng 2016;14:59–88. https://doi.org/10.1007/s10518-015-9811-5.
[68] Gautam D. Observational fragility functions for residential stone masonry buildings in Nepal. Bull Earthq Eng 2018;16:4661–73. https://doi.org/10.1007/s10518-018-0372-2.